NOISE EFFECTS ON WAVE-GENERATED TRANSPORT INDUCED BY IDEAL WAVES

JUAN M. RESTREPO AND GARY K. LEAF

ABSTRACT. We consider the transport velocity in boundary layer flows driven by either noisy monochromatic progressive or standing waves. The central issue addressed here is whether such flows are capable of sustaining a transport velocity when noise is present in the wave field and, if so, in what ways the noise affects the transport velocity, the mean wall shear stress, and the total mass flux.

Specifically, we address the effect of noise due to unresolved processes. Our study is motivated by the fact that in the natural setting it is the norm rather than the exception that noise is present in the wave field. We find that when noise is added to standing waves, the transport in the boundary layer leads to a nonzero mass flux. On the other hand, noise due to progressive waves reduces the mass flux. Further, we find that the drift velocity will have two components: a deterministic one and a diffusive one.

1. INTRODUCTION

The theoretical framework of wave-generated motion in the context of water, acoustic, and plasma waves rests on the fact that under certain conditions of motion the Lagrangian particle paths do not describe closed orbits and thus, over time, the particles that make up the fluid

Date: July 28, 1999.

1991 *Mathematics Subject Classification.* 65N60.

Key words and phrases. unsteady boundary layer, wave-generated transport, mass transport, drift velocity, Stokes drift, wave-induced transport.

This work was supported in part by the Mathematical, Information, and Computational Sciences Division subprogram of the Office of Advanced Scientific Computing Research, U.S. Department of Energy, under Contract W-31-109-Eng-38. This work was performed while JMR was a summer Faculty Research Program visitor of the Mathematics and Computer Science Division at Argonne National Laboratory and a Computational and Applied Mathematics/Program in Computing visiting faculty member at UCLA. Funding of the Beowulf-class cluster on which the calculations were performed was made possible by a grant from the University of Arizona.

itself will drift. Perhaps the earliest theoretical studies of this phenomenon are those of Stokes [1] and Lord Rayleigh [2], thus making this a research topic that is nearly 150 years old. In the 1950s Longuet-Higgins [3] derived an asymptotic expression for the mean Lagrangian velocity in an oscillating laminar boundary layer. He also demonstrated that boundary layers, however thin, have a dramatic effect on the ensuing drift generated by waves. Further, he suggested that this type of wave-generated motion could be important in the transport of sediment and, by extension, in the transport of pollutants and nutrients. Johns [4] and Longuet-Higgins [5] showed that the situation is not qualitatively dissimilar in the case of a mixing-length-type boundary layer (for a review see [6], [7] and references contained therein). Streaming due to the oscillation of immersed objects in a fluid or the oscillation of bounding surfaces is also well documented and of considerable interest in the engineering community; it is now a classic topic in fluid mechanics monographs and textbooks (see [8]).

On the theoretical side, a geometrical interpretation of the relation between the averages in the Lagrangian and the Eulerian frames led Andrews and McIntyre to formulate a generalized Lagrangian mean theory of wave-generated transport [9], [10], a theory in which certain geometrical properties of the flow are preserved, such as Kelvin's circulation.

Progressive waves induce a steady transport velocity in a uniform channel (see [6]). On the other hand, a standing wave field has the potential of producing a steady spatial structure in a tracer field occupying a boundary layer. This fact is exploited in models [11], [12] for the formation and evolution of large-scale sandbar structures (see [13] and [14] for reviews). Wave-generated transport has been shown to modify the dynamics of interacting flows. A consequence of momentum and continuity conservation is that short waves are dynamically modified by the mass and momentum fluxes due to finite amplitude long waves [15], [16]. The interaction of currents with the streaming induced by a wave field has been shown to generate circulation cells, which have a striking resemblance to Langmuir cells in the ocean and the atmosphere [17], [18], and has been shown to modify the Ekman boundary layer in rotating flows [19]. It has also been suggested as an important transport mechanism in oceanic flows relevant to climate dynamics [20] and in the shallow reaches of the continental shelf where waves and currents interact in a significant way [21].

In this study we consider the effect of idealized noise on the transport generated by monochromatic progressive or standing waves. Noise in this study is understood to represent underresolved processes in the

external forcing. When a flow is forced by standing waves, we show that Gaussian noise, manifesting itself as statistical perturbations of the phase and amplitude of the waves, generates a nonzero total mass flux in the boundary layer. We also show that when the forcing is due to progressive waves, noise significantly diminishes the mass flux.

Elucidating ubiquitous aspects of wave-generated transport, even in an idealized setting, sheds light on the motion of tracers acted upon by waves in the physical setting. The particles affected by this transport mechanism may be passive tracers; they may be mechanically interacting particles such as sand, self-propelled biological organisms, or pollutants that interact mechanically and chemically. Often, these particles, in turn, affect the flow in the boundary layer, such as is the case in a loose sedimentary bed. Our study does not focus on the dynamics of these particle systems, although we make use of passive tracers to investigate the transport velocity itself.

We use a Prandtl model to approximate the flow in the boundary layer in the neighborhood of an ideally smooth bounding wall (see [22]). As shown in [23], the flow under the action of waves in the boundary layer in a wave channel with a perfectly smooth bottom is well captured by the progressive-wave solution of the linear Prandtl boundary layer equations[1]

$$u_1 = \cos(kx - \omega t) - \exp(-\beta z)\cos(kx - \omega t + \beta z), \tag{1}$$

where u_1 denotes the horizontal velocity, k is the wavenumber and ω the frequency of the wave, x is the horizontal coordinate and z the vertical coordinate, t is the time, and $\beta \equiv \omega z_h/\sqrt{(2\nu)}$, where ν is the dissipation and z_h is the boundary layer thickness. For the standing wave case the solution to the linear Prandtl equations is

$$\begin{aligned} u_1 &= \cos(kx)\cos(\omega t) \\ &\quad - \exp(-\beta z)\cos(kx)\cos(\omega t - \beta z). \end{aligned} \tag{2}$$

In this study, however, we do not use these expressions in the computation of the transport. Instead, we use numerical means to obtain the approximate solution to the nonlinear Prandtl model.

Section 2 focuses on a description of the ideal wave channel and on details of the Prandtl boundary layer model and its numerical approximation. A description of how the transport velocity relates to the properties of the flow appears in Section 3. In this section, we also review some salient aspects of the transport velocity in boundary layer

[1]These equations are more commonly known as "Stokes's second problem." Since Stokes's name is invoked in several places and in different contexts, however, we will call these equations the linear Prandtl equations to avoid possible confusion.

flows forced by either progressive or standing waves in the absence of noise. The former produces a steady drift velocity with nonzero mean and no spatial structure, the latter a steady drift velocity with zero mean and spatial structure. We think of the progressive wave and the standing wave cases as being two extremes in the transport they generate. The simplest external forcing that generates a nonzero mean as well as spatial structure in the steady drift is a "leaky" standing wave. In this case the external forcing can be characterized by waves with an incident and a reflecting component that has a relative amplitude $0 < R < 1$. As a function of R the mass transport characteristics of this flow were explored in detail in [24]. Examination of these three examples leads to an understanding of how noise affects the transport when it is present in the external forcing The situation when noise is present is considered in Section 4. Conclusions relevant to wave-generated transport derived from this work appear in Section 5.

2. Description of the Ideal Wave Channel

The horizontal coordinate in the computational domain, or "channel," is denoted by x and the vertical coordinate by z. The $z = 0$ plane coincides with the bottom of the channel, which is assumed to be ideally smooth and rigid. The channel is taken to be periodic in x and three wavelengths long.

The relation between the angular frequency ω and the wavenumber k for the waves is assumed to be

$$\omega^2 = gk\tanh(kh),$$

where g is the gravity constant and h is the water column depth.

The size of kh is a determining factor in the penetration depth of these waves; in particular, if kh is small, we expect the penetration depth of the waves to be significant. This is relevant to mass transport in the boundary layer because its strength is determined to a large extent by the amplitude of the forcing immediately outside the layer. A small kh value implies that the waves are long compared with the depth of the water column. In the simulations to be discussed presently, $kh \approx 0.2534$. The period P of the waves was 8 seconds, producing a wavenumber 0.2534 m^{-1} corresponding to waves with a wavelength of approximately $\lambda = 24.79$ m.

The forcing velocity immediately outside of the boundary layer is denoted by $U(x,t)$. In the experiments the velocity amplitude was $U_m \approx 0.7456$ m/s. The external forcing velocity was either a progressive or a standing wave (denoted PW and SW, respectively), with a

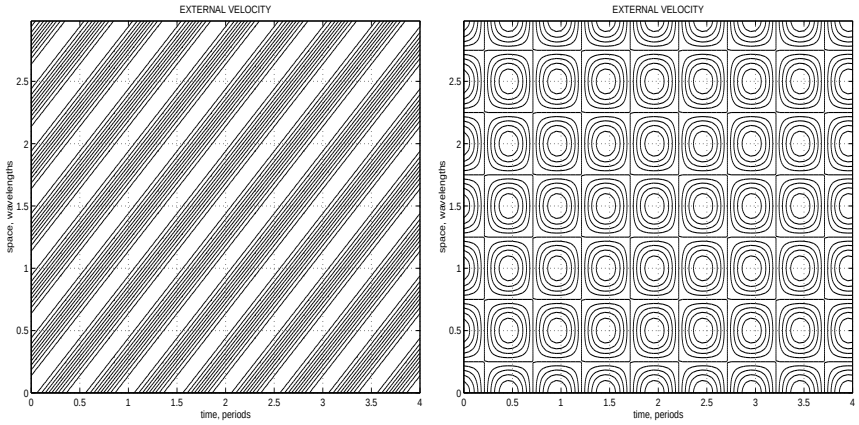

FIGURE 1. External forcing velocity $U(x,t)$: (a) progressive wave case, (b) standing wave case. See text for a description of the forcing velocity amplitude, wavelength, and frequency.

phase that may have depended on time. The progressive wave forcing velocity was

$$U(x,t) = U_m \cos(kx - \omega t - \gamma(t)), \tag{3}$$

with k determined by the dispersion relations given above, once ω was chosen in the experiment. The *phase noise* γ is a time-dependent Gaussian noise process with zero mean. The noise source has two parameters: the *noise amplitude*, which is related to the variance of the process, and its *frequency*, denoted by $1/T_n$, where T_n is given in units of fractions of a period P of the forcing. The noise frequency determines how often the external forcing is perturbed.

The standing wave forcing was of the form

$$U(x,t) = U_m \cos(kx)\cos(\omega t - \gamma(t)). \tag{4}$$

Figure 1 depicts the space-time contours of the forcing velocity. Shown here is the external velocity during the last four periods of a numerical experiment. The contours correspond to the absolute value of the velocity amplitude. Since the forcing is oscillatory, the velocity will reverse direction during each cycle. For reference, Figure 2 shows the effect noise has on the PW external forcing. Figure 2a shows the external forcing when the phase is perturbed randomly at times shorter than the period of oscillation of the external forcing ($T_n = P/20$). Figure 2b shows the external forcing when the perturbations to the phase are made at times commensurate with the period. In both figures the noise amplitude is 0.1π.

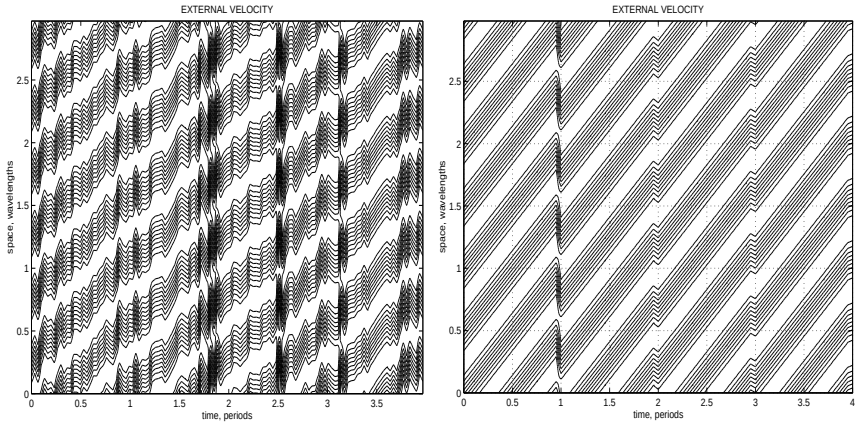

FIGURE 2. External forcing velocity $U(x,t)$ with added noise, for the progressive wave case: (a) phase noise perturbations at times shorter than the period ($T_n = P/20$), (b) noise perturbations at times equal or longer than the period ($T_n = P$). The parameters are the same as in Figure 1. Noise amplitude is 0.1π.

2.1. **Boundary Layer Model and Its Numerical Approximation.** The Prandtl equations are

$$\frac{\partial u}{\partial t} + \epsilon u \frac{\partial u}{\partial x} + \epsilon w \frac{\partial u}{\partial z} - \frac{S^2}{Re}\frac{\partial^2 u}{\partial z^2} = U_t + \epsilon U U_x \tag{5}$$

$$u_x + w_z = 0, \tag{6}$$

where the following scaling has been used: $x \leftarrow x/\lambda$, $z \leftarrow z/\delta$, $t \leftarrow t\omega$, $u \leftarrow u/U_m$, $w \leftarrow w/W_m$, with $W_m \equiv U_m\delta/\lambda$, $U \leftarrow U/U_m$, with $new \leftarrow old$, new being the dimensionless variables. Here, $\delta \equiv \sqrt{\nu/\omega}$ is the Stokes layer thickness, and ν is the dynamic viscosity of water.

The dimensionless numbers $\epsilon = 1/S$, where $S = \omega\lambda/U_m$, and $Re = \omega\lambda^2/\nu$ characterize the flow. These are $S \sim 10^3$ and $Re \sim 10^7$ in all the experiments reported in this study.

The flow was made periodic at the far and near ends of the channel. A no-slip boundary condition was applied at the channel wall, and the velocity at the edge of the boundary layer matched the external forcing velocity $U(x,t)$. In the numerical experiments the flow was initialized by using the analytical solution to the linear Prandtl equations, that is, the solution to the mass and momentum conservation equations with all terms proportional to ϵ in (5) set to zero.

A full description of the discretization of the equations appears in Appendix A. The appendix also details how the results derived by using the Prandtl model and its numerical approximation compare with those

obtained by using a numerical solution of the Navier-Stokes equations under the same physical conditions. Since running averages will play an important role as a diagnostic tool in what follows, in Appendix B we provide the particulars of our tests on the accuracy of the algorithm used. Running averages were computed after discarding the first three periods of the simulation, thereby removing the effect of the initial state of the channel flow on the resulting averages. The simulations that produced the data for the analysis were carried out for a sufficiently long time to establish an approximation of the asymptotic behavior of the flow and diagnostic quantities. In each group of simulations the actual length of the runs is explicitly given; however, figures featuring the drift or the transport in space and time will show the flow only during the last four time periods of the experiment. To assay the characteristics of the transport velocity under different wave forcing and noise conditions, we also used an algorithm to advect tracers, thus obtaining approximations of the Lagrangian paths of ideal tracers. The advection algorithm is described in detail in Appendix C.

3. The Transport Velocity

We wish to investigate the mean Lagrangian velocity $\langle \mathbf{u}_L \rangle$ because this quantity is related to the transport of tracers in the flow. The angled brackets denote the mean: for some quantity $f(\cdot, t)$, say, the mean at time T is defined as

$$\langle f(\cdot, T) \rangle \equiv \frac{1}{T} \int_{t_0}^{t_0+T} f(\cdot, t)\ dt.$$

Here, t denotes time, and t_0 is the time at which the average is initiated. This definition of the mean applies to both periodic and nonperiodic quantities and is frequently used to compute a mean of experimental or field data.

The connection between the mean Lagrangian velocity and the mean Eulerian velocity may be expressed as $\langle \mathbf{u}_L \rangle = \langle \mathbf{u}_E \rangle + \tilde{\mathbf{u}}$, with $\langle \mathbf{u}_E \rangle$ representing the averaged Eulerian velocity. We will refer to $\langle \mathbf{u}_E \rangle$ as the *drift velocity*. In this study, prominence is given to the drift velocity because it is a robust measurable diagnostic quantity for the mass flux. The drift velocity is also important because it is related to the average shear stress, which in turn is related to such factors as the characterization of forces required to dislodge and/or initiate particle tracer motion in a flow. Since the average shear stress is

$$\langle \rho \nu \frac{\partial u}{\partial z}|_{z=0} \rangle,$$

it is approximately equal to the drift velocity, in the neighborhood of the bottom, times $\rho\nu/\delta$, where ρ is the density, ν the viscosity, and δ the layer thickness.

Direct calculation of the mean Lagrangian velocity everywhere in the boundary layer is impractical, and thus it is difficult to obtain the transport velocity. Since the calculation of the drift velocity is straightforward, however, an approximation to the transport velocity is possible if a good representation of the term $\tilde{\mathbf{u}}$ is available. In oscillatory flows such as those considered here, it is possible to approximate $\tilde{\mathbf{u}}$ by taking a finite number of terms in the series expression as derived in [3]. For smooth boundary layer flows, the particle orbits do not close on themselves; and if the distance between the starting and the ending points over the period is small, an adequate approximation to $\tilde{\mathbf{u}}$ is obtained by retaining a small number of terms in the expansion. The first term in that expansion is

$$\mathbf{u}_S = \langle \mathbf{S} \cdot \nabla \mathbf{u}_1(\cdot, t) \rangle,$$

where $\mathbf{S} = \int^t \mathbf{u}_1(\cdot, t')\, dt'$. Usually $\mathbf{u}_S$ is called the Stokes drift velocity (see [7]). Hence, if higher-order terms in the expansion of $\tilde{\mathbf{u}}$ are sufficiently small, the *transport velocity* may be well approximated by $\langle \mathbf{u}_E \rangle + \mathbf{u}_S$. Retaining only one term in the expansion of $\tilde{\mathbf{u}}$ may be supported by the following argument. We write $\mathbf{u} = \mathbf{u}_1 + \mathbf{u}_2 + \cdots$ and $\langle \tilde{\mathbf{u}} \rangle = \mathbf{u}_S + \langle \tilde{\mathbf{u}}_2 \rangle + \cdots$. The time average of $\mathbf{u}_1$ is zero, since it is the solution to the linear Prandtl boundary layer equation. We surmise that

$$\langle \tilde{\mathbf{u}}_2 \rangle = \left\langle \int^t \mathbf{S}(\cdot, t') \cdot \nabla \mathbf{u}_1(\cdot, t')\, dt' \cdot \nabla \mathbf{u}_1(\cdot, t) + \frac{1}{2} \mathbf{S}(\cdot, t) \cdot \nabla^2 \mathbf{u}_1(\cdot, t) \cdot \mathbf{S}(\cdot, t) \right\rangle.$$

An estimate of the size of $\mathbf{u}_S$ in terms of the magnitude of the velocity U_m, the wavenumber k, and the frequency ω of the size of the Stokes drift is $\mathbf{u}_S = \mathcal{O}(U_m^2 k/\omega)$. Similarly, an estimate of $\langle \tilde{\mathbf{u}}_2 \rangle$ is $\mathcal{O}(U_m^3 (k/\omega)^2)$. The ratio of $\langle \tilde{\mathbf{u}}_2 \rangle$ to $\mathbf{u}_S$ is thus $\mathcal{O}(U_m k/\omega)$, which is small in all cases considered in this study (approximately 10^{-2}).

Since we are studying aspects of the transport in a thin boundary layer whose aspect ratio is very small when compared with the horizontal spatial scales, we will speak of the horizontal component of the transport velocity as the transport velocity itself.

Ideal tracers in a flow move away from locations along the channel that are subject to high transport velocities and tend to concentrate at locations where the transport velocity amplitude is low, leading to an uneven distribution of tracers. If the transport velocity is steady,

however, this distribution will be uniform along the channel. The horizontal direction in which the tracers move is given by the sign of the horizontal component of the transport itself. A useful qualitative characterization of the flow is afforded by thinking of the transport, at any time, as composed of a (spatial) mean, or DC, and a fluctuating, or *residual*, component.[2] The spatial mean naturally corresponds to the lowest component of the space Fourier spectrum and describes the net transport current. More important, the quantity $1/3\lambda_l \int_0^{3\lambda_l} \langle \mathbf{u}_L \rangle \, dx$, which is the total mean flux per unit length of fluid in the channel, is proportional to the DC. The remaining portion of the spectrum makes up the residual component of the transport velocity. This residual transport is important because, if it is steady or nearly steady in time, it implies the existence of spatial structure in the transport and the potential for a nonuniform mean distribution of tracers under the action of the flow.

Let us suppose for the moment that the DC is zero and that steady running average conditions prevail. Then tracers at locations where the residual transport is zero do not move. We call these locations *traps*. An accumulating trap, or *node*, is one in which there is a zero in the residual and, in addition, the transport locally has a negative slope that persists over time. These traps attract moving particles, and accumulation ensues at these sites. If the DC component is not zero, however, the net transport is a result of the DC and the residual components. In this case, particles accumulate at the traps only if the tracers have some threshold of motion higher than the mean but lower than the maximum magnitude of the transport.

3.0.1. *Transport Induced by Progressive and Standing Waves.* Next we summarize some qualitative differences between the transport velocity induced by progressive and standing wave external forcing in the absence of noise.

Figure 3 shows the space-time plot of the horizontal component of the transport velocity. Figure 3a corresponds to PW and Figure 3b to SW forcing, respectively. The velocity was measured roughly a Stokes layer depth above the wall. The figures depict the contours of the velocity amplitude, with the dark and light patches corresponding to low and high velocities, respectively. The amplitude of the velocity may be inferred from Figure 5. At any particular position along the channel, the transport (which is defined in terms of a running average) exhibits oscillatory behavior and a slowly decaying envelope. This is

[2]We emphasize that the terms DC and residual apply only to spatial considerations, not time dependencies.

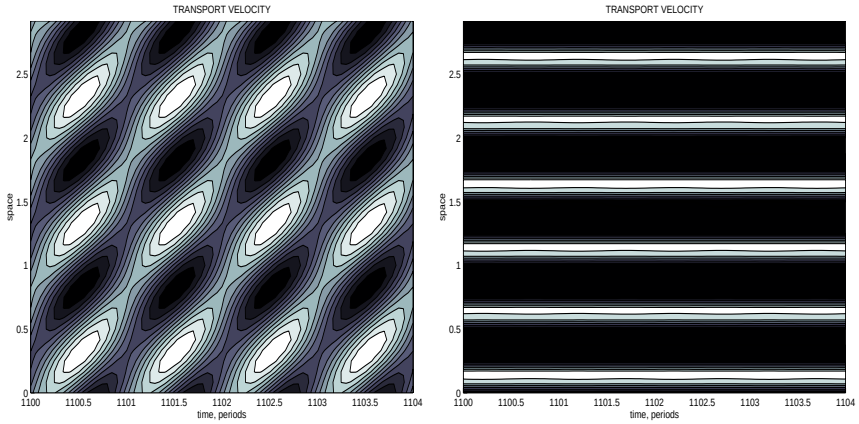

FIGURE 3. Contours of the transport velocity (horizontal component) due to (a) progressive waves (PW), (b) standing waves (SW). The vertical scale is comparable to that of Figure 5.

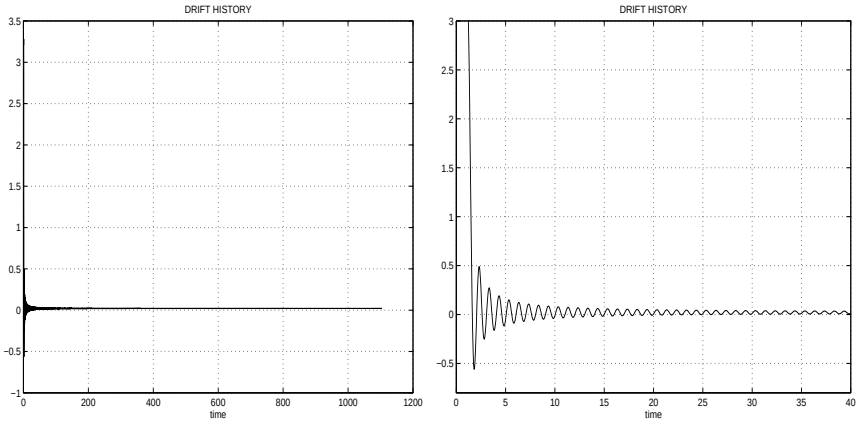

FIGURE 4. Time history of the drift velocity at some particular position in the channel for the PW case with no added noise: (a) detail during the first few periods of the simulation, (b) full history. See Figure 5 for a vertical scale for the amplitude of the transport velocity at the end of the experiment.

illustrated in Figure 4, for the PW case. For these monochromatic, time-harmonic waves, the *mean* transport is numerically equal to the value of the transport itself at times commensurate with the period of the forcing. Our calculations show that the mean transport agrees with standard theory (see [25, pp. 353–364] and [6, pp. 420–434]). That is, for waves progressing from left to right, the mean transport

for PW forcing is steady in time and uniform in space. Its magnitude is nonzero and positive. Figures 5a and 5c portray the transport at the end of the experiment, for the PW forcing case, in the absence of noise. Figure 5c shows the superposition of the transport velocity for the last few periods. The spatially fluctuating traces in this figure depict the transport velocity at times incommensurate with the period. Traces that are constant across the entire channel correspond to the mean transport. These latter ones are colinear and depict the mean transport velocity.

For SW forcing, the transport is steady in time. It is composed of spatial cells with horizontal dimensions half the wavelength of the forcing. The spatial mean of the transport for the SW case in the absence of noise is zero. The SW transport with no noise present is shown in Figure 3.

With the aid of these figures we can construct a qualitative description of how ideal or passive tracers[3] would respond to the transport velocity under PW forcing in the absence of noise. The space and time symmetries induced by the sinusoidal forcing imply that the mean transport must be constant. Intuitively, this reflects the fact that as the wave train progresses down the channel, it imparts the same effect on the flow everywhere along the channel. If the transport at some given height above the wall, locally, is found to have a specific value, symmetry implies that the transport measured anywhere else along the channel must be the same, provided that the averaging process required in computing the transport is well defined. Indeed, this fact is reflected by our computation. The transport is constant and is always positive. Since the transport is positive, passive tracers would advect in the direction of wave motion, toward the end of the channel. Clearly, the tracer flux is proportional to the spatially averaged transport, which in this case is equal to the transport itself, and hence the flux is also positive and constant. Furthermore, since the mean wall shear stress is proportional to the drift velocity, the bottom of the tank would experience, on average, a positive and uniform mean shear stress. These findings agree with the standard asymptotic theory.

For the SW case, the situation can be summarized as follows. The spatial mean of the transport is found to be machine zero; therefore, the mean flux is zero as well. However, the SW flow produces a transport with steady spatial structure, proportional to $\sin(2kx)$. Thus, passive tracers will move away from locations of high transport and tend to concentrate at locations where the transport velocity amplitude is

[3]As the name implies, ideal tracers trace the Lagrangian path in a flow.

zero, forming the cells that the asymptotic theory predicts. While the total flux is zero, for the noiseless SW case, ideal particles with initial position corresponding to one of the transport cells will stay in that cell for all time.

When the flow is forced by monochromatic progressive waves, nodes are not found in the transport, since the residual transport is zero. This follows from the observation that, for progressive waves in a uniform channel, the model is translationally invariant. Tracers will move in the direction of the progressive waves because the DC component is nonzero and positive. In the SW case, however, nodes do occur because the DC component is zero and the residual has time-steady traps with negative slopes.

4. The Effect of Noise in the Forcing on the Transport

Noise usually is present both in the laboratory and in the natural setting. Since wave-generated transport is typically a relatively weak phenomenon, one expects noise to have a significant effect on it, especially over the long time frames required for significant transport to occur. Our investigation focuses on how the transport and, by extension, the mass flux and the mean shear stress are affected by noise derived from unresolved physical processes.

In the context of the boundary layer problem it is reasonable to suggest that noise perturbations affect either the phase or the amplitude of the wave forcing and that the boundary layer itself would respond according to (5) and (6). At any instant in time, noise perturbations would induce an uncertainty in the measurements of the actual location of maxima and minima in the wave, as well as an uncertainty in the measurement of the wave amplitude.

Models for the PW and SW forcing that incorporate the above qualities are (3) and (4). ¿From these expressions it is clear that a nonzero $\gamma(t)$ will affect both the phase and the amplitude of the forcing. With $\gamma(t)$ a Gaussian noise process, with zero mean, the resulting model is one in which the uncertainty in the phase and the amplitude of the wave grows proportional to the square-root of time. The adoption of Gaussian statistics is done here in an ad hoc way. However, this assumption is often invoked (and sometimes abused) in order to characterize the statistics of a great many oceanic processes.

Intuitively, it seems natural to think that phase noise acts as an effective decorrelator of running averages, since the noise would act as some sort of diffusive process. Indeed, our results bear this out. However, it is difficult to envisage in what way noise actually affects such aspects of the flow as the transport, the wall shear stress, and the

mass flux. For example, does the transport slowly decay, completely disappear, destabilize, or develop a totally different structure?

Two properties characterize the noise fluctuations: the amplitude and the frequency. These become parameters in our experimental study on the effect of noise on transport. The amplitude is related to the wave uncertainty in phase. The frequency is related to how often a noise perturbation occurs. It affects the coherence of the external forcing over time; the lower the frequency, the higher the degree of spatial coherence, but the longer it takes for quantities calculated via running averages to nominally settle. There is a space-time symmetry, so that noise perturbations in time, affecting the whole extent of the wave, correspond to perturbations in space, affecting the wave for a long period of time. Hence, the effect of the noise over time at a single place has a corresponding description in terms of the effect of noise over some span of the channel at some particular instant in time.

In each experiment the code was run for 150 periods. Measurements, however, were made only in the last 100 periods of the run. We summarize below the outcome of experiments in which the noise amplitude was varied in a range $0 - \pi$. Coverage of the noise frequency parameter range was less complete. We did, however, test noise frequencies that were both higher and lower than the frequency of external forcing.

For the PW case, noise caused the DC, and thereby the mass flux, to drop appreciably, compared with the noiseless case. The DC was no longer steady. The residual was also modified by the presence of noise, becoming amplified significantly. In fact, ignoring the DC component, we note an interesting qualitative change on the drift velocity due to noise, namely, the appearance of nodes in the residual. These nodes are not traps for ideal tracers, however, since the residual is everywhere positive. Hence, although the transport is structured, a nonzero flux will be present everywhere along the channel. If ideal tracers were present, they would eventually reach the end of the tank, regardless of where in the tank they were placed. On the other hand, if the tracers had some threshold of motion slightly above the DC level, it would then be possible for tracers to accumulate at the nodes.

The most salient structural changes in the drift due to noise are evidenced in Figure 5. In Figure 5a contours of the drift velocity, noise absent, are portrayed in space and time. For comparison, Figure 5b shows the case when noise is present. To emphasize their symmetry, we have not shaded the contours; however, it is understood that in 5a they would be consistent with Figure 3a, and that in Figure 5b the contours would appear as alternate shaded and unshaded regions. In fact, from Figure 5b it is seen that when noise is present the residual

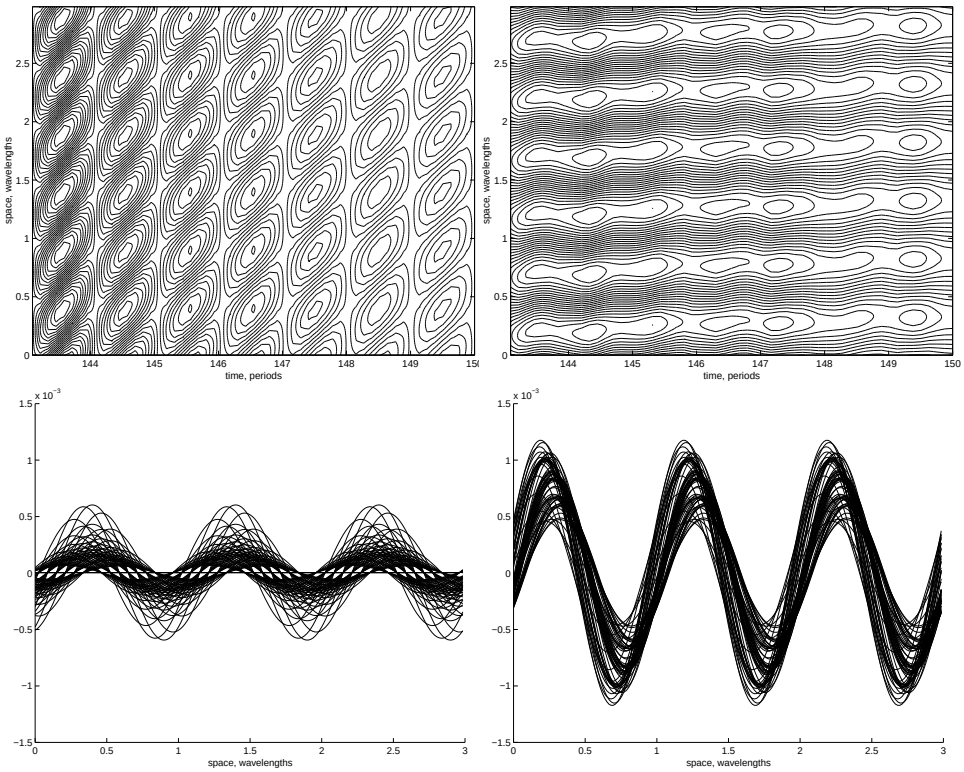

FIGURE 5. Effect of noise on the drift velocity, PW case. The space-time plot of the drift velocity: (a) no noise, (b) with noise. The superposition of the drift velocity over the last 10 periods of the simulation, as a function of position along the channel: (c) no noise, (d) with noise. Noise frequency: $1/T_n = 20/P$; noise amplitude: 0.5π.

flow has a nearly steady structure in time. Figures 5c and 5d shows a superposition of the drift for the last ten periods of the run, as a function of position. Figure 5d, which corresponds to the case in which noise is present, clearly shows that the running averages are nonuniform in space and nearly steady in time. Examination of the residual in both cases depicted in Figure 5 reveals that the transport in the noisy case has a significantly lower DC component than does the noiseless counterpart, and a residual that is not present in the noiseless case.

Thus we find that for the PW case, the presence of noise has two significant effects on the drift. First, the magnitude of the mean drift is greatly reduced. Second, the residual flow acquires a nearly steady spatial structure. These effects are not as sensitive to the amplitude or

frequency of the noise but, rather, to the existence of a noise perturbation.

For the SW case, noise has a less dramatic but nevertheless significant effect. Whether noise is present or not, the space-time picture of the transport looks very similar to that of Figure 3. This is certainly true for small but reasonable amplitudes of the noise. The residual is affected by the appearance of fluctuations inside the trapping cells. The cases with noise and with no noise present are depicted in Figures 6a and 6b, respectively. Of note is the absence of the periodic appearance of a reverse flow in each of the cells of the standing wave structure in the noisy case. This is evidenced by comparing it with the noiseless case in Figure 6. Examination of the data reveals that in the absence of noise the DC is zero and thus the total flux is zero. With noise present, however, the flux is nonzero and unsteady, sometimes even becoming negative. Summarizing the findings on the SW experiments, we find that noise induces a small nonzero total flux.

Next we quantify the dependence of the transport velocity on the noise amplitude and frequency. Specifically, we calculate the Lagrangian trajectories (for details, see Appendix C), using both the vertical and horizontal components of the Eulerian velocity. As Figures 7-10 indicate, the vertical component of the velocity is very small compared with the horizontal component. Furthermore, by virtue of (6) we can infer that for the PW case the vertical velocity forms cells of upward and downward directed motion and that in these cells the vertical velocity must be monotonic. Thus we expect that particles will exhibit both a transverse and an upward or downward trend in their motion, when acted upon by the velocity field in the layer.

The result of calculating the Lagrangian trajectories, over nine periods of forcing, appear in Figure 7. The particles were placed initially at equally spaced horizontal intervals, roughly one Stokes layer above the wall. The path traced by a particle in the noiseless PW case appears in Figure 7a, its noisy counterpart in Figure 7b. The noise amplitude and frequency were 0.5π and $20/P$, respectively. The dissipation inherent in the advection scheme is apparent in the figures by a trend in the orbit to get smaller in radii. This causes the particle to get deflected slightly in the vertical direction. The effect is fairly small, however, when compared with the particles' reaction to the total velocity field. Overall, the result of these two is slight: note the aspect ratio of the vertical and horizontal coordinates on the plots.

When the particle paths are sampled at times commensurate with the period and their tracks connected by lines we obtain Figure 8a, and Figure 8c, for the noiseless and noisy case, respectively. Figure

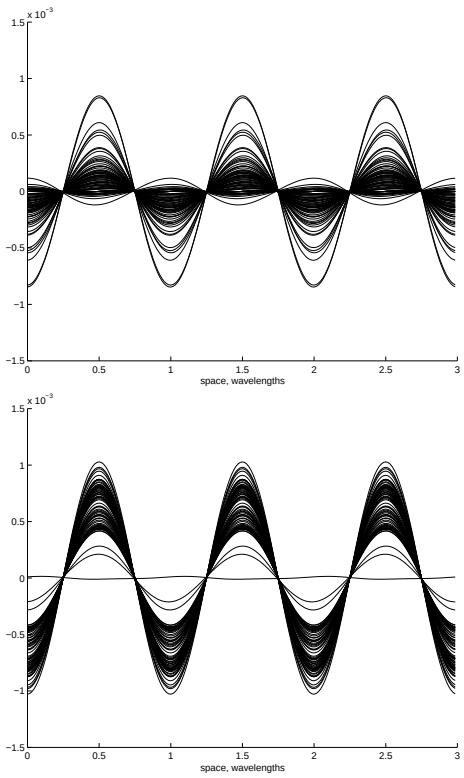

FIGURE 6. SW case. Superposition of the drift velocities, at many times corresponding to the last periods of the simulation, as a function of position along the channel: (a) no noise, (b) with noise. Noise frequency: $1/T_n = 20/P$; noise amplitude: 0.5π.

8b and Figure 8d show the starting and final position particle position along the channel for these two cases. ¿From this figure it is clear that the particles are not traveling as far along the channel in the presence of noise, and that the horizontal component of the velocity is greatly affected, thus making the relative effects of the vertical component of the velocity on the particle motion more prominent.

How this manifests itself in the flux can be assessed by the direct calculation of the flux at some given location in the channel. By counting particles traveling from left to right across $x = 1.2\lambda$, say, as positive and those traveling from right to left across $x = 1.2\lambda$ as negative, we can arrive at a net flux value. The choice of location was arbitrary in this calculation. Figures 9a and 9b show the flux of tracers for the PW noiseless and noisy case, respectively. Clearly, the noise reduces the net flux significantly.

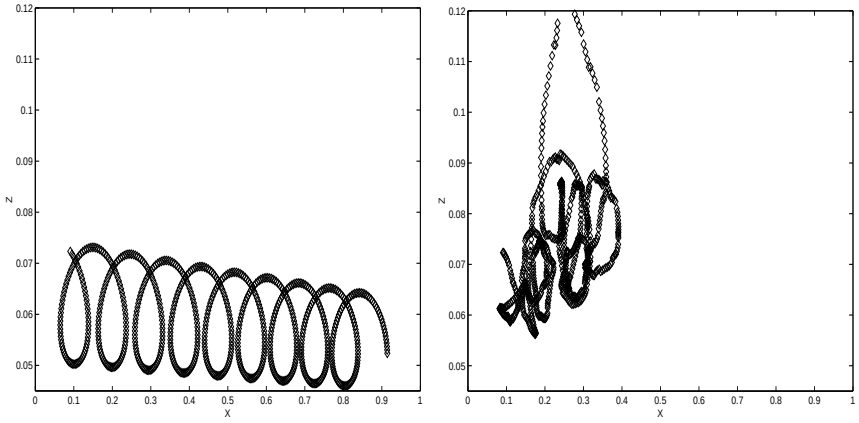

FIGURE 7. Lagrangian particle trajectories: (a) no noise, (b) noise, with frequency $20/P$ and amplitude 0.5π. PW case.

As we said previously, the most salient effect of noise on the SW case is the creation of a small net flux. This is borne out in the Lagrangian trajectories shown in Figures 10a and 10b, which correspond to the noiseless and noisy case, respectively. As is evident from the noisy case, tracers leak from cell to cell.

Next we show how the flux is affected by the noise amplitude and the frequency. The quantitative dependence of the flux on the presence of noise is examined by the following proxy calculation. We calculate the statistical mean displacement of a particle over a fixed time. We then use this data to calculate a transport velocity and thus obtain the flux.

Ensemble averages of the Lagrangian trajectory are computed. Each member of the ensemble corresponds to the trajectory of one of thirty-three different release times, over the period of the forcing wave. Hence, each particle is released at a different phase value of the wave. Furthermore, for any given Lagrangian path identified by a given initial phase, we calculate a path under three different noise time series. Among these three realizations the parameters of noise amplitude and frequency are the same. When no noise is present, the three trajectories are identical. With noise, the three trajectories starting with an initial phase have no commonality in their time series. In fact, removal of the deterministic component of all the trajectories shows that the ninety-nine Lagrangian paths are unique realizations that share only statistical properties. As before, the total time of each run is nine periods, and settings for the experiments are the same as in Figure 8, save for variations in the noise frequency and amplitude.

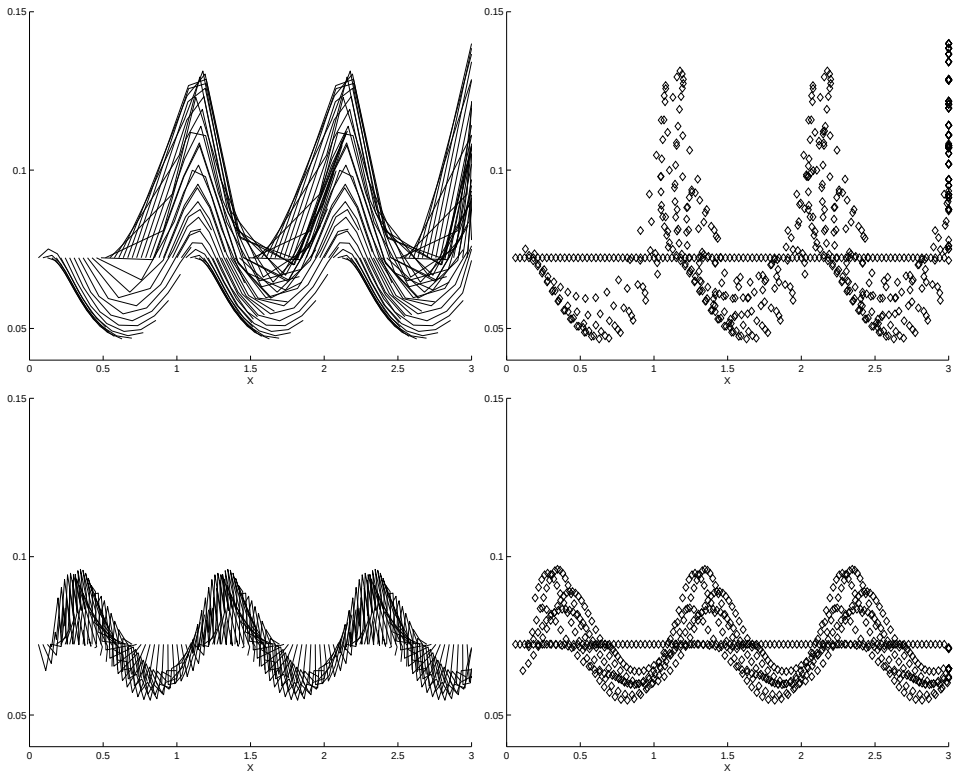

FIGURE 8. Effect of noise on the Lagrangian trajectories, PW case: (a)–(b) no noise, (c)–(d) with noise. Trajectories were sampled at times commensurate with the period. Noise frequency: $20/P$; noise amplitude: 0.5π. The initial and final particle positions are shown in (b) and (d).

The procedure just described yields the ensemble average unsigned *distance*, which is defined as $|\overline{\mathbf{x}_f - \mathbf{x}_i} \cdot \overline{\mathbf{x}_f - \mathbf{x}_i}|$, where the subscript f denotes the mean particle position after nine periods and i the initial position. We also report on the *displacement*, which we define to be the unsigned distance

$$\max_{0 \le T \le 9P} |\overline{\mathbf{x}(T) - \mathbf{x}_i} \cdot \overline{\mathbf{x}(T) - \mathbf{x}_i}|,$$

where P is one period. The distance will thus measure the average distance an ideal tracer in the fluid would move in nine periods, and the displacement the relative scatter of the position of the tracer over this time span. Both the distance and the displacement are in units of fractions of a wavelength.

The results of this experiment are tabulated in Table 1. In the PW

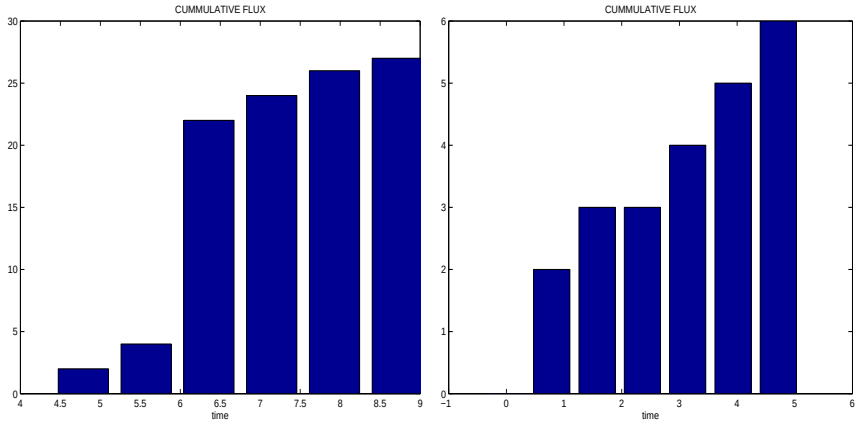

FIGURE 9. Lagrangian particle fluxes at $x = 1.2\lambda$, PW case: (a) no noise, (b) noise. Note the different vertical scales. Noise frequency: $20/P$; amplitude: 0.5π. Experimental conditions are the same as in Figure 8.

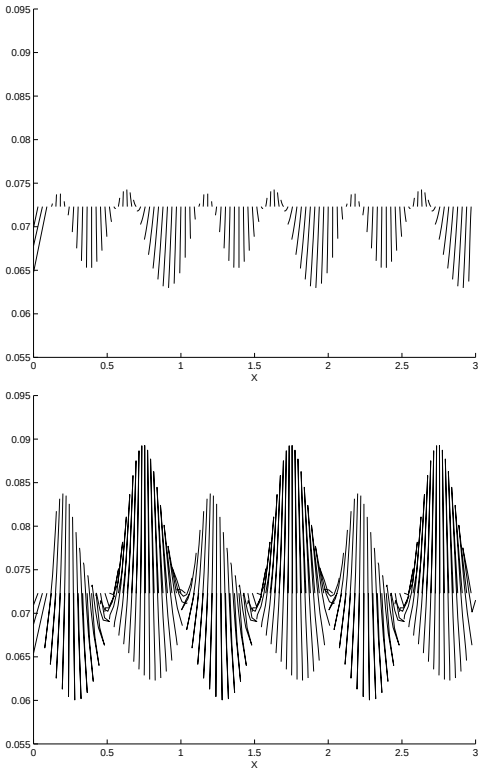

FIGURE 10. Particle trajectories sampled at times commensurate with the period, SW case: (a) no noise, (b) noise. Noise frequency: $20/P$; noise amplitude: 0.5π.

TABLE 1. Relative displacement (D) and distance (d) of ensemble trajectory as a function of the noise amplitude (N). Noise frequency is $1/20P$, total time: 9 periods.

Progressive Wave			Standing Wave		
N	D	d	N	D	d
0.0	0.9806	0.9806	0.0	0.0196	0.0000
0.1	0.9242	0.9242	0.1	0.0228	0.0084
0.3	0.6098	0.5817	0.3	0.0717	0.0005
0.5	0.4546	0.4546	0.5	0.5033	0.3230
0.7	0.2989	0.2943	0.7	0.0639	0.0101
0.9	0.2455	0.2440	0.9	0.0164	0.0033

case the table shows that noise reduces the flux by significantly diminishing, on average, particle advection. A fit of the data shows that the distance drops nearly linearly with noise amplitude. The drop in the displacement is strikingly similar to the distance, indicating that the particle, on average, gets further away the longer the forcing is active, regardless of the amount of noise, and that on average the maximum displacement is well captured by the distance itself. In the SW case, the data indicates that the presence of noise increases the average distance and displacement of ideal tracers as the noise amplitude increases, provided that the noise amplitude is small. When the amplitude of the noise is large, however, the distance and the displacement drop. Since the noise has zero mean and is Gaussian, the results indicate that for large noise levels the noise itself largely determines the flux in the SW case. Moreover, the discrepancy between the displacement and the distance indicates that, on average, particles do not attain maximum displacement at the final time. Transport in the large noise amplitude regime is then diffusion dominated.

The noise frequency dependence of the displacement and the distance is straightforward, given a fixed noise amplitude. It speaks more about the measurement process itself than about the physics. Our comments are limited to the effect of the noise frequency on the outcome, for frequencies significantly higher than the forcing frequency. Our findings indicate that the transport magnitude and shape are not influenced greatly by the change in noise frequency, regardless of whether the forcing is PW or SW. The slow convergence of the running averages, however, means that as the frequency of the noise decreases, the running averages of the monitored quantities take longer to converge to within some small tolerance. When the duration of the experiments is increased in indirect proportion to the noise frequency, the results

become statistically similar, particularly in the PW case. Significant changes occur because of the presence or absence of noise, rather than the noise frequency value itself.

5. Conclusions

The transport velocity and the mass flux are associated with the time-averaged Lagrangian velocity and thus are important in the dynamics of tracers in a fluid flow. For waves of finite amplitude, the transport velocity may be approximated by the superposition of the mean Eulerian velocity and the Stokes drift. In this study we explored how the transport velocity in a laminar boundary layer, bounded by an ideal straight wall, under the action of sinusoidal progressive or standing waves, is affected by noise. The highly idealized setting of our experimental configuration enabled us to compare the effect of the noiseless situation—which is well known—with that of the noisy situation.

We specifically addressed how noise from underresolved dynamics affects the transport, the mean shear stress, and the fluxes in a laminar boundary layer. For our numerical simulations we purposely used measuring techniques that are commonly used in a laboratory or field setting. The boundary layer asymptotic theory, though of limited validity, is entirely appropriate for the perfectly smooth channel that we used in our experiments. Nevertheless, as a further check, we benchmarked our results qualitatively to a direct numerical simulation of the Navier Stokes equations in the channel and found very good agreement. In summary, our results may show (acceptable) quantitative differences with what we think of a generally agreed-upon model for fluids, and may show only mild qualitative differences.

The noise perturbation applied in this problem was Gaussian with zero mean. The noise perturbation produces monotonic slow growth in the uncertainties in the wave amplitude and phase that accumulate over time.

We found that noise has a dramatic and somewhat unexpected effect on the transport velocity in the boundary layer and, by extension, on the mean wall shear stress and the mass flux. Our general organizing principle has been to examine how noise affects two naturally occurring situations: when the forcing external to the layer is a progressive wave (PW) and when the forcing is a standing wave (SW). The asymptotic theory for the deterministic problem shows that these two forcing cases may be viewed as two extremes in the outcome on the transport in the natural setting. In fact, with these extremes it is easy to envision, at least qualitatively, how the situation for the leaky wave will play out

(in this endeavor we are helped by the calculations of the deterministic case by Carter et al. [24]).

The findings in this study suggest that the transport resulting from PW and SW external forcing subject to noise due to underresolved processes may be characterized by two components: a deterministic one and a diffusive one. Their relative effect on the transport depends on whether the external flow is PW or SW.

In the PW case, noise in the forcing decreases the mean and the total mass flux. The spatial mean wall shear and the transport velocity also decrease. At the same time, there is an enhancement of the spatially nonhomogeneous portion, or residual, of the transport velocity and thus of the wall shear stress. The mean flux drops almost linearly with the noise amplitude. Nevertheless, the mean flux is still positive, and thus ideal tracers present in the flow still will move in the direction of the waves, but at a reduced rate compared with the noiseless case. In the event that these tracers have a threshold of motion greater than the spatial mean of the transport but smaller than the maximum transport, the tracers may produce a nonuniform spatial distribution along the channel. With respect to the frequency of perturbations, the results are more telling about the measurement process itself. For noise frequencies that are higher than the forcing frequency, the running averages of quantities such as drift velocity and transport tend to require more time in reaching an adequate level of convergence. The reason is that these running averages converge at a rate inversely proportional to time, weighted by the period of the forcing. If the running averages are taken over commensurably longer time periods, the lower the noise frequency is made, the closer they reach statistical equivalence, all other things remaining the same. This assumes, of course, that the time steps in the numerical calculation are sufficiently small that the noise signal is adequately resolved.

In the SW case it is found that noise induces a very small mass flux. This mass flux can be in either direction along the horizontal coordinate of the channel. Hence, the spatial mean of the transport tends to increase slightly at the expense of the residual. Overall, however, the SW case shows that the structure and the magnitude of the transport changes when noise is present, but is relatively insensitive to increases in the noise amplitude or noise frequency. Compared to the PW case, the Lagrangian path of the SW case displays more statistical scatter. That is to say, in the PW case it is found, on average, the mean orbit displacement tends to be closely related to the beginning and average ending particle position, over a specified time span. In contrast, the

maximum displacement for the SW case does not usually agree with the average ending particle position.

Appendix A. Numerical Approximation of the Wave Channel

Solutions to (5) and (6) may be approximated by using finite-difference techniques. The spatial domain of the periodized wave channel had dimensions $0 \leq x < 3\lambda$, where λ is the wavelength of the external forcing, and $0 \leq z \leq z_h$. In the horizontal direction, we use an equally spaced grid with coordinates given by $x_j = j\Delta x$, where Δx is fixed; the grid levels in the z direction were distributed according to

$$z_k = (k/K)^p, \tag{7}$$

where p is a real value between 1 and 2, K is the total number of grid levels in z, and $0 \leq k \leq K$. The triplet $(j, k; p)$ uniquely determines any position in the channel. The discrete domain is denoted by $\Omega = (x_j, z_k)$.

The finite-difference approximation of the equations of fluid motion on Ω was accomplished by splitting the hyperbolic and parabolic parts in a standard way (see Hirsch [29]). The hyperbolic part was advanced in time explicitly by using a low-order upwinding scheme. The parabolic part marched forward in time by using a Crank-Nicholson scheme. First and second derivatives with respect to z were approximated as

$$\frac{\partial f}{\partial z} \approx \frac{1}{(\Delta + \nabla) z_i} \left(\frac{\nabla z_i \Delta f_i}{\Delta z_i} + \frac{\Delta z_i \nabla f_i}{\nabla z_i} \right),$$

where $\Delta f_i = f(\cdot, z_{i+1}) - f(\cdot, z_i)$, $\nabla f_i = f(\cdot, z_i) - f(\cdot, z_{i-1})$, and

$$\frac{\partial^2 f}{\partial z^2} \approx \frac{2}{(\Delta + \nabla) z_i} \left(\frac{\Delta f_i}{\Delta z_i} - \frac{\nabla f_i}{\nabla z_i} \right),$$

respectively, for some dynamic quantity f.

The accuracy was evaluated by comparing the computed solution with an exact solution. The test problem was Stokes's second problem, which describes the boundary layer flow over a horizontally oscillating plate [22, p. 93]. The external forcing was set to the horizontal velocity at the edge of the layer $u(x, 1, t) = \cos(\omega t)$. The exact solution of Stokes's second problem, for z_h sufficiently large, is $u(z, t) = \exp(-s(1 - z)) \cos[\omega t - s(1 - z)]$, where $s = \sqrt{2/\omega}$. In the test results to be presented, the forcing frequency was set to $\omega = 2\pi$ and the wavenumber to 6π, which produces a wavelength $\lambda = 1/3$. The equations were integrated for five periods, at which time the analytic and computed results were compared. Quadratic convergence was

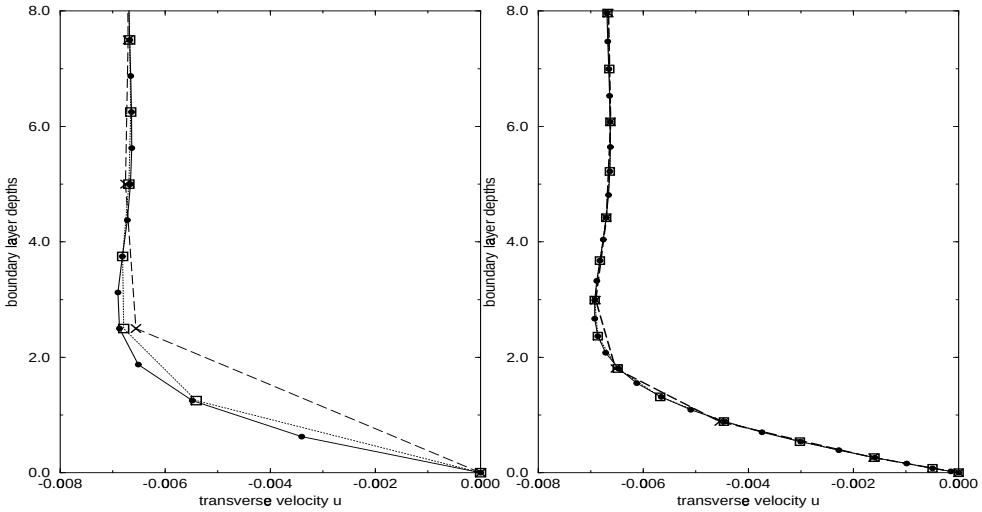

FIGURE 11. The computed horizontal velocity u at a fixed location x_j, as a function of depth, for different values of K; at some location x, after five periods of oscillation: (a) uniform mesh, with $p = 1$; (b) nonuniform mesh, with $p = 1.75$. Notation: crosses, $K = 20$; squares, $K = 40$; dots, $K = 80$.

achieved when the grid was uniform in z. For nonuniform grids, the convergence was superlinear.

Figure 11 shows cross sections of the computed horizontal velocity u as a function of z at a fixed location x_j. The units of the z axis in the figure are given in terms of boundary layer thicknesses δ. The external velocity was a progressive wave of dimensionless amplitude 0.006. Figure 11a shows the velocity, as approximated by using a uniform grid ($p = 1$ following (7). The $K = 20$ case is depicted by crosses, the $K = 40$ case by squares, and the $K = 80$ case by dots in the figure. All cases were computed with $M = 90$ and $\Delta t = 2\pi/800$. The graph shows the computed solutions converging in accordance with our expectations of what a typical layer profile should look like. Figure 11b shows the computed velocity profiles at the same position in x_j and same time as in Figure 1a, but these solutions were computed on a variable mesh (again following (7)) with $p = 1.75$. It is clear from these figures that the nonuniform mesh adequately captures the solution, using fewer discretization points than would otherwise be required with a uniform grid. Furthermore, $\Delta x = \lambda/66$, and the time step was set to $\tau/400$, where τ is the period of the forcing.

For the flows investigated in this study the mean shear stress is proportional to the mean Eulerian velocity. Unlike the mean Eulerian

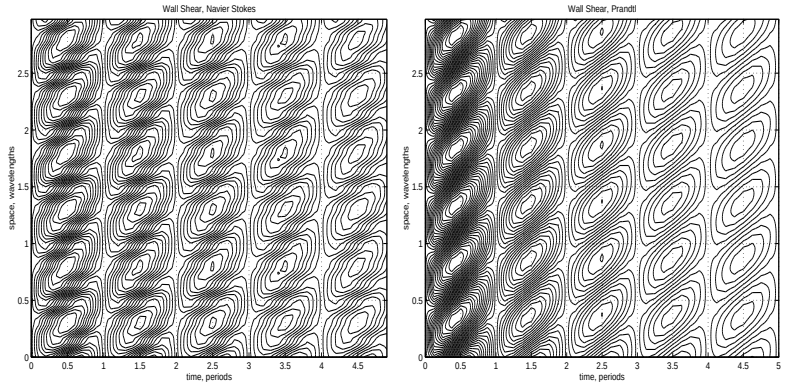

FIGURE 12. Wall shear stress: (a) Navier-Stokes, (b) Prandtl.

velocity, however, the mean shear stress depends only on the channel length and time. Hence, it is a quantity that lends itself to answer the following question: Do the results obtained by using a Prandtl model differ qualitatively (and in an appreciable way, quantitatively) from those obtained by using the Navier-Stokes equations? We benchmarked the mean shear stress computed by using a spectral element Navier-Stokes (NS) solver due to Fischer (see [30] for details). The solver uses periodic boundary conditions at the far and near ends of the channel and no-slip conditions at the bottom of the channel. The forcing

$$\begin{aligned} u &= U_m \cos(kx - \omega t) \cosh(ky) / \sinh(kh) \\ v &= U_m \sin(kx - \omega t) \sinh(ky) / \sinh(kh) \end{aligned}$$

generates a bulk pressure field that drives the flow. The initial condition is also derived from the above forcing. In the comparisons, aspect ratios reached in the Prandtl code were not accessible in the NS code. Instead of parameters used in the experiments reported in this study, the comparison of the time-averaged wall shear stress was made by using $h = 0.01$ m depth, $\omega = 2\pi$, and $U_m = 0.2h\omega$ m/s. The comparison is made at $t = 8$ s. The NS solver was run by using eight cells in the z direction and eighteen in the x direction, and the elements used polynomials of order 8. Under progressive wave forcing, the asymptotic wall shear stress $\langle (\partial u/\partial z)|_{z=0} \rangle$ reported by the NS solver is approximately 10.7 s^{-1}, whereas the shear is 3.41 s^{-1} for the Prandtl model code. Given that there is no exact description of how thick the boundary layer should be, for the numerical computation of solutions in the Prandtl model, the quantitative comparison indicates adequate agreement. Qualitative agreement can be inferred from Figure 12.

Appendix B. Testing the Running-Average Algorithm

Running averages were used extensively as a diagnostic tool in this study. In particular, running averages were used to calculate the mean Eulerian velocity. The running averages were tested as follows. A sinusoidal progressive wave $\cos(kx - \omega t)$ replaced the velocity field within the Prandtl code. All other aspects of the code remained the same, including the running average routine itself. The running average output of the code was then examined at times commensurate with the period, over many tens of thousands of time steps. At these times, the outcome for the running average of this sinusoidal signal was machine zero throughout the channel length, as expected.

Appendix C. The Advection Scheme

In addition to characterizing the flow under different forcing and noise conditions, we were also interested in assessing how the flow itself affects the distribution of passive tracers present in the boundary layer. To do this, we used a tracer tracking algorithm. The algorithm yields the eventual distribution of a collection of ideal tracers that are initially placed uniformly along the length of the channel and then subjected to advection by the transport velocity.

Specifically, the computed Eulerian velocity $\mathbf{u}(x_j, z_i, t_n)$, $n = 0, 1, \ldots$, and $t_n = n\Delta t$, was used to compute $\mathbf{U}_T(x, z, t_n)$, a first-order splined semidiscrete interpolation of the advection velocity. This advection velocity was assumed fixed for a time interval $T\Delta t$, where $T \geq 1$. N_p particles were distributed uniformly along the channel, at locations $\mathbf{X}_k(t_0)$, where $k = 1, 2, \ldots, N_p$, at some height z_i, at the initial time t_0. We then allowed the particles to advect according the the local velocity $\mathbf{U}_T$. Hence, particles moved to a new position $\mathbf{X}(t_n + T\Delta t) = T\Delta t \mathbf{U}(\mathbf{X}_{t_n}, t_n)$ in time $T\Delta t$. The new advection velocity was then calculated and the procedure repeated to find the new position of the particles.

Since the magnitude of the velocities was small, freezing both the particle velocity and position for T steps yielded a saving in computational expense. The value of T in the experiments reported here was 5. This value increases the dissipation inherent in the advection algorithm. Hence, particle orbits, even for a perfectly linear acoustic field, would exhibit drift and thus not close on themselves. Drift, in turn, leads to overestimates in the particle transport. Hence, particle advection experiments must be short in duration and particle flux comparisons made in relative, rather than absolute, terms.

REFERENCES

[1] G. G. Stokes, "On the theory of oscillatory waves", *Philosophical Transactions of the Royal Society of London* 8 (1847), 441.

[2] Lord Rayleigh, "On waves", *Philosophical Magazine* 5 (1876), 257–279.

[3] M. S. Longuet-Higgins, "Mass transport in water waves", *Philosophical Transactions of the Royal Society of London* 245 (1953), 535–581.

[4] B. Johns, "On the Mass Transport Induced by an Oscillatory Flow in a Turbulent Boundary Layer", *Journal of Fluid Mechanics* 60 (1970), 177–185.

[5] M. S. Longuet-Higgins, "The mechanics of the boundary layer near the bottom in a progressive wave ", *Proceedings, 6th Conference on Coastal Engineering* (1958).

[6] C. C. Mei, *The Applied Dynamics of Ocean Surface Waves*, World Scientific, Singapore, 1989.

[7] O. M. Phillips, *The Dynamics of the Upper Ocean, 2nd edition*, Cambridge University Press, Cambridge, 1977.

[8] D. O. Telionis, *Unsteady Viscous Flows*, Springer-Verlag, New York, 1981.

[9] D. G. Andrews & M. E. McIntyre, "An exact theory of nonlinear waves on a Lagrangian-mean flow", *Journal of Fluid Mechanics* 89 (1978), 609–646.

[10] M. E. McIntyre, "A note on the divergence effect and the Lagrangian-mean surface elevation in periodic water waves", *Journal of Fluid Mechanics* 189 (1988), 235–242.

[11] J. M. Restrepo & J. L. Bona, "Model for the formation of longshore sand ridges on the continental shelf", *Nonlinearity* 8 (1995), 781–820.

[12] J. M. Restrepo, "Behaviour of a sand ridge model", *European Journal of Mechanics B/Fluids* 6 (1997), 835–861.

[13] J. Fredsoe & R. Deigaard, *Mechanics of Coastal Sediment Transport*, World Scientific, Singapore, 1992.

[14] J. F. A. Sleath, *Sea Bed Mechanics*, John Wiley and Sons, New York, 1984.

[15] M. S. Longuet-Higgins & R.W. Stewart, "Changes in the form of short gravity waves on long waves and tidal currents", *Journal of Fluid Mechanics* 8 (1960), 565–583.

[16] M. S. Longuet-Higgins & R.W. Stewart, "The changes in amplitude of short gravity waves on steady non-uniform currents", *Journal of Fluid Mechanics* 10 (1961), 529–549.

[17] A.D.D. Craik & S. Leibovich, "A rational model for Langmuir circulations", *Journal of Fluid Mechanics* 73 (1976), 401–426.

[18] J. C. McWilliams, P.P Sullivan & C.H. Moeng, "Langmuir turbulence in the ocean", *Journal of Fluid Mechanics* 334 (1997), 1–30.

[19] N. E. Huang, "On surface drift currents in the ocean", *Journal of Fluid Mechanics* 91 (1979), 191–208.

[20] J. C. McWilliams & J. M. Restrepo, "The wave-driven circulation", *Journal of Physical Oceanography* 29 (1999), 2523–2540.

[21] J. M. Restrepo, "Wave-current interactions in shallow waters and shore-connected ridges", *Continental Shelf Research* 21, 1331–1360.

[22] H. Schlichting, *Boundary Layer Theory*, McGraw-Hill, New York, 1987.

[23] J. F. A. Sleath, "Velocity measurements close to the bed in a wave tank ", *Journal of Fluid Mechanics* 42 (1970), 111–123.

[24] T. G. Carter, P. Liu & C. C. Mei, "Mass transport by waves and offshore sand bedforms", *Journal of Waterways, Harbours, Costal Engineering Division ASCE* 99 (1973), 165–184.

[25] G. K. Batchelor, *Introduction to Fluid Dynamics*, Cambridge University Press, Cambridge, 1988.

[26] O. S. Madsen, "Mass transport in deep-water waves", *Journal of Physical Oceanography* 8 (1978), 1009–1015.

[27] W. D. Grant & O. S. Madsen, "Combined wave and current interaction with a rough bottom", *Journal of Geophysical Research* 84 (1979), 1797–1808.

[28] W. D. Grant & O. S. Madsen, "The continent-shelf bottom boundary layer", *Annual Review of Fluid Mechanics* 18 (1986), 265–305.

[29] C. Hirsch, *Numerical Computation of Internal and External Flows, Vols I & II*, John Wiley and Sons, New York, 1990.

[30] P. F. Fischer & A. T. Patera, "Parallel simulation of viscous incompressible flows ", *Annual Review of Fluid Mechanics* 26 (1994), 483–528.

Mathematics Department, and Program in Applied Mathematics, University of Arizona, Tucson, AZ 85721, U.S.A.
E-mail address: restrepo@math.arizona.edu
URL: http://www.math.arizona.edu/~restrepo

Mathematics and Computer Science Division, Argonne National Laboratory, Argonne, IL 60439, U.S.A.
E-mail address: leaf@mcs.anl.gov